Supporting Information

Unveiling the synergic Potential of Dual Junction $MoSe_2$/n-Ga_2O_3/p-GaN Heterojunction for Ultra-Broadband Photodetection

Vishnu Aggarwal[abc], Manish Kumar[d], Rahul Kumar[ab], Sudhanshu Gautam[ab], Aditya Yadav[ab], Shikha Shrivastava[ab], Anjana Dogra[ab], Govind Gupta[ab], Sumeet Walia[c], Sunil Singh Kushvaha[ab]*

*

[a] CSIR-National Physical Laboratory, Dr. K. S. Krishnan Road, New Delhi 110012, India

[b] Academy of Scientific and Innovative Research (AcSIR), Ghaziabad 201002, India

[c] School of Engineering, RMIT University, Melbourne, Victoria 3000, Australia

[d]Physics Department and CSMB, Humboldt-Universität zu Berlin, Zum Großen Windkanal

2, 12489 Berlin, Germany

Corresponding Author Email: kushvahas@nplindia.org

Figure S1 displays the evolution of RHEED patterns of PLD-grown samples GS and GT during growth. Figures S1 (a) and S1 (b) show the RHEED image of thermally cleaned sapphire (0001) and p-GaN/sapphire (0001). The absence of diffuse scattering or streaks in the RHEED image confirms that the surface is free from defects or impurities and is smooth and uniform. In Figures S1 (c) and S1 (d), the changes in spacing and intensity of the typical RHEED pattern (after 200 laser shots of Ga_2O_3) from that of thermally cleaned sapphire (0001) and p-GaN template suggest the formation of a new crystal structure. The RHEED images in Figure S1 (c) and S1 (d) are observed to be along [102] and [010] directions of Ga_2O_3, respectively [1]. The streaky RHEED pattern suggests that initially, Ga_2O_3 started to grow in 2D growth mode. On the other hand, the spotty RHEED pattern shown in Figures S1 (e) and S1 (f) along both [102] and [010] directions indicates that 3D Ga_2O_3 has been grown using the PLD technique after the final growth. To examine the surface morphology of grown samples, we conducted AFM scanning and Figures S1 (g) and S1 (h) display the obtained AFM scanned images of the PLD-grown samples GS and GT, respectively, with a scan area of $(2\ \mu m)^2$. The AFM image of sample GS revealed the formation of a granular β- Ga_2O_3 thin film on sapphire (0001). The root mean square (RMS) roughness of sample GS was estimated to be 7.29 nm for a scan area of $(2\ \mu m)^2$. On the other hand, the AFM image of sample GT showed that a granular island type β- Ga_2O_3 thin film had grown on a p-GaN template, which had a few small pits on the surface. The RMS roughness of the film was estimated to be 4.78 nm.

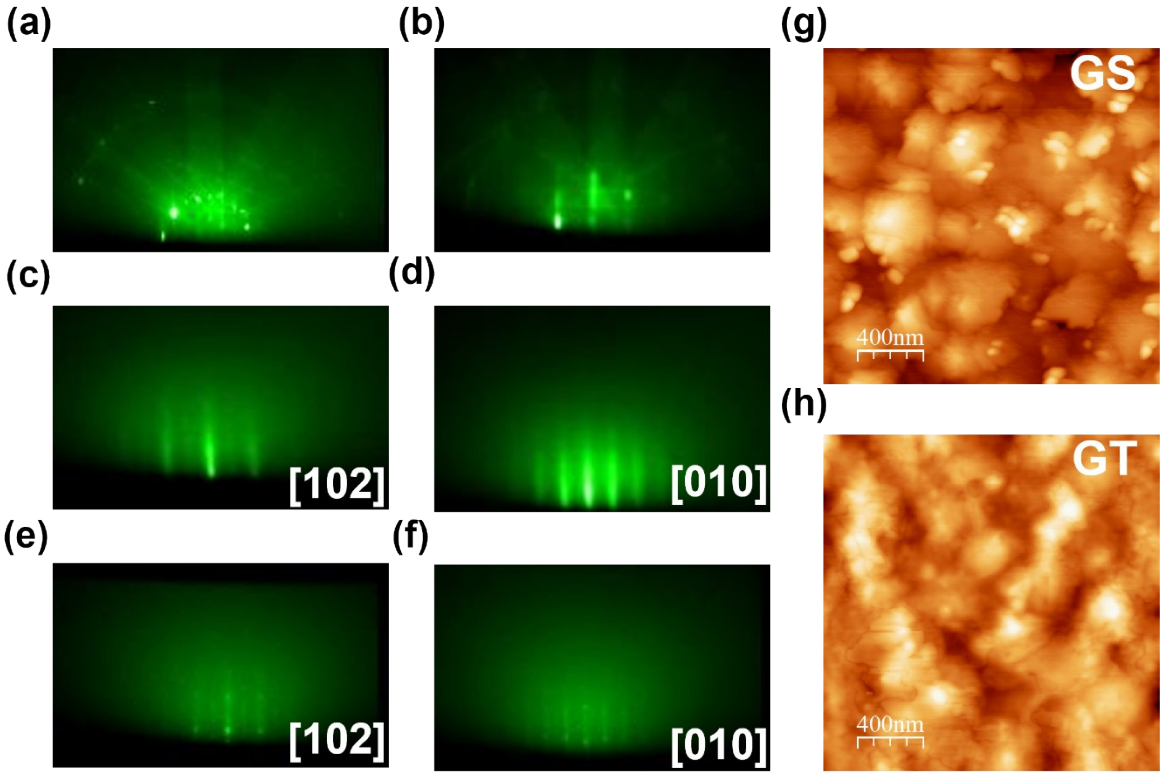

Figure S1: *RHEED pattern of (a) and (b) thermally cleaned sapphire (0001) and p-GaN template, respectively (c) and (d) during growth of Ga_2O_3 after 200 laser shots, (e) and (f) after final growth of Ga_2O_3 and (g) and (h) displays the AFM image of sample GS and sample GT, respectively.*

Figure S2 (a) represents the Lorentzian-fitted PL spectrum, showing an intense emission peak at 2.8 eV and an emission peak at 3.0 eV. These peaks were reported to correspond to the dominating donor-acceptor pair (deep donor level induced due to nitrogen-vacancy and acceptor level due to Mg doping of 6×10^{16} cm^{-3}, i.e., Mg_{Ga}) and free-to-bound exciton pair recombination [2]. The schematic of the energy band diagram for various transitions of electrons in the p-GaN template is shown in Figure S2 (b). The XPS N 1s core level scan was performed for the pristine p-GaN template and after the growth of Ga_2O_3 on the p-GaN template, as shown in Figures S2 (c) and S2 (d), respectively. The N 1s spectra are deconvoluted to three peaks where highly intense peaks at 395.7 eV [Figure S2 (c)] and 397.09 eV [Figure S2 (d)] are attributed to the N-Ga bond in pristine GaN and Ga_2O_3/GaN, respectively. The presence of other peaks at lower binding energy reveals the presence of the

Ga LMM Auger signal [3]. It was noticed that Auger signals diminished after the growth of Ga_2O_3, as shown in Figure S2 (c). Further, Figure S2 (e) shows the valence band spectra of samples GS and GT in the 0-15 eV binding energy range. Furthermore, the valence band spectrum of pristine p-GaN has been presented in Figure S2 (f), which reveals that the Fermi level in the p-GaN template is only 0.64 eV, far from its valence band maxima.

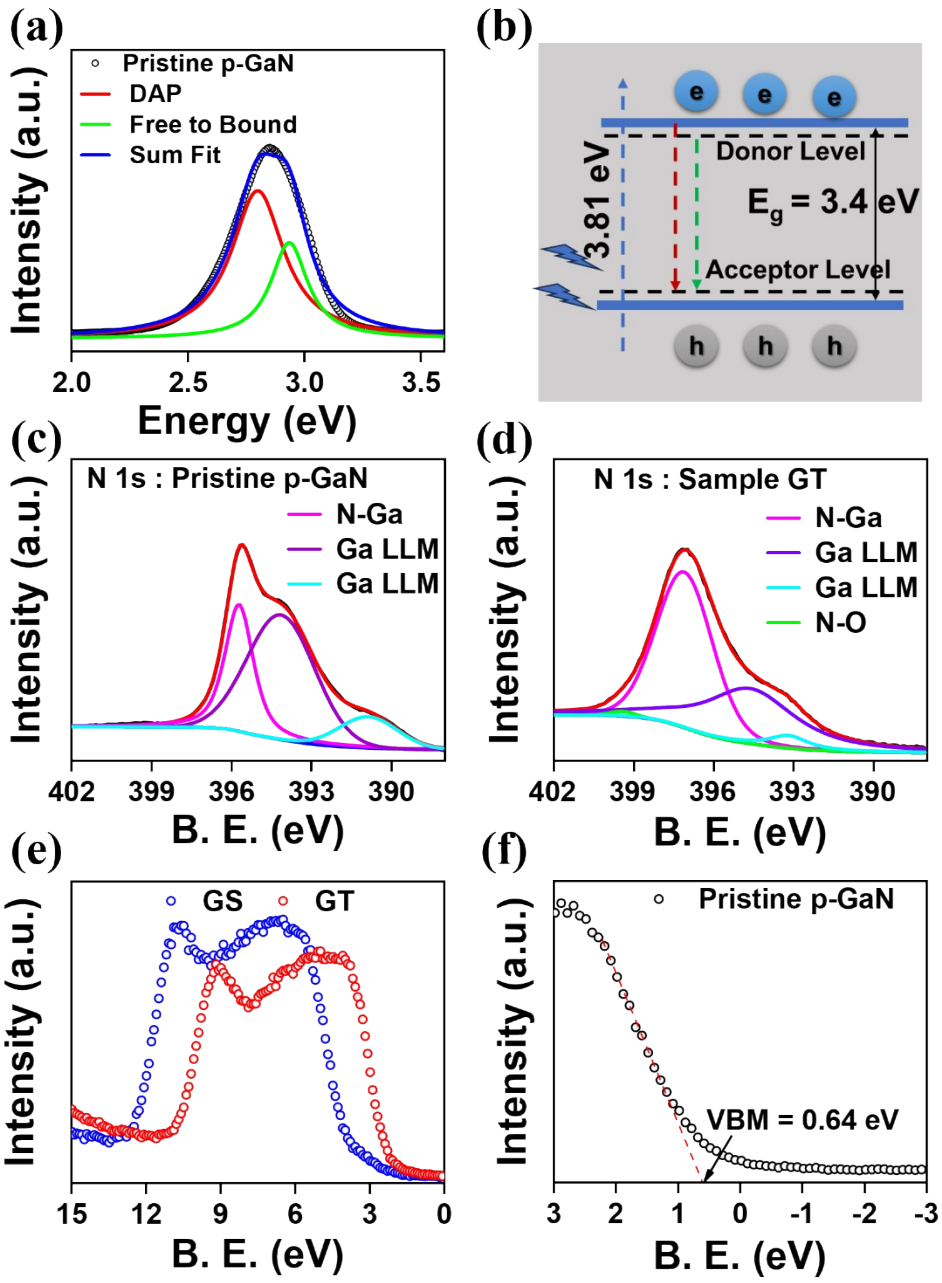

Figure S2: *(a) Lorentzian fitted PL spectra, (b) Energy band diagram of various transitions of electrons in p-GaN template. N 1s core-level scan of (c) pristine p-GaN and (d) sample GT, (e) broad-range valence band spectra of samples GS and GT, and (f) pristine p-GaN.*

Computational Details

We used a *tight* setting with a *tier* 2 basis set for all atomic species. The self-consistency loop was converged with a total energy threshold of 0.01 meV. All the structures were fully relaxed using PBESol functional until the forces were smaller than 0.001 eV/Å. A 1 × 3 × 2 supercell (120-atom), which is the replication of a unit cell (20-atom), was used to make the defect localized in the system. A 4 × 4 × 4 *k*-grid was used for Brillouin zone integration.

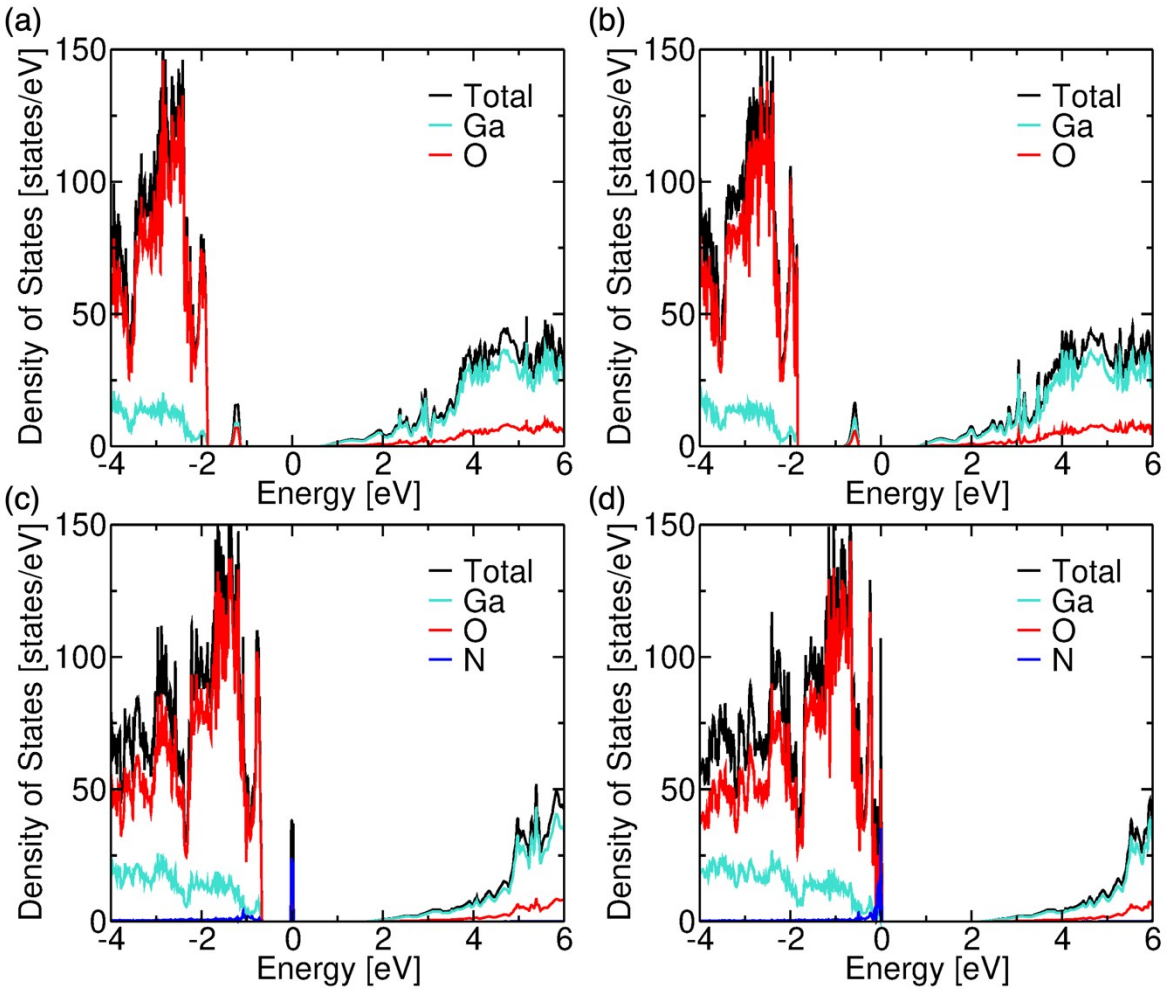

Figure S3: *Atom projected partial density of states of (a) an O-vacancy at O1-site, (b) an O-vacancy at O2-site, (c) N-substitution at O1-site and (d) N-substitution at O2-site in* Ga_2O_3.

Next, we fabricated MSM PD to compare the photo response quality of the PLD-grown Ga_2O_3 samples GS and GT. The schematic diagrams of the PD fabricated on PLD-grown Ga_2O_3 are shown in Figures S4(a) and S4(b). To understand the behavior of the fabricated devices, we

performed the current-voltage (I-V) characteristics of each PD device under dark in the voltage range of -10 to 10 V, as shown in Figure S4 (c). The sub-linear I-V curves reveal the formation of a semi-ohmic type of metal-semiconductor junction. The difference between the work function of Au (5.1eV) and the electron affinity of Ga_2O_3 (4 eV) leads to an energy barrier at the metal-semiconductor interface, resulting in semi-ohmic I-V characteristics. The dark current of the devices is in milliamperes, which can be attributed to surface states and mid-gap states formed in Ga_2O_3 semiconductors, which are predicted theoretically by DFT calculations and perceived experimentally from PL spectra in Figure 3 and Figure 1, respectively.

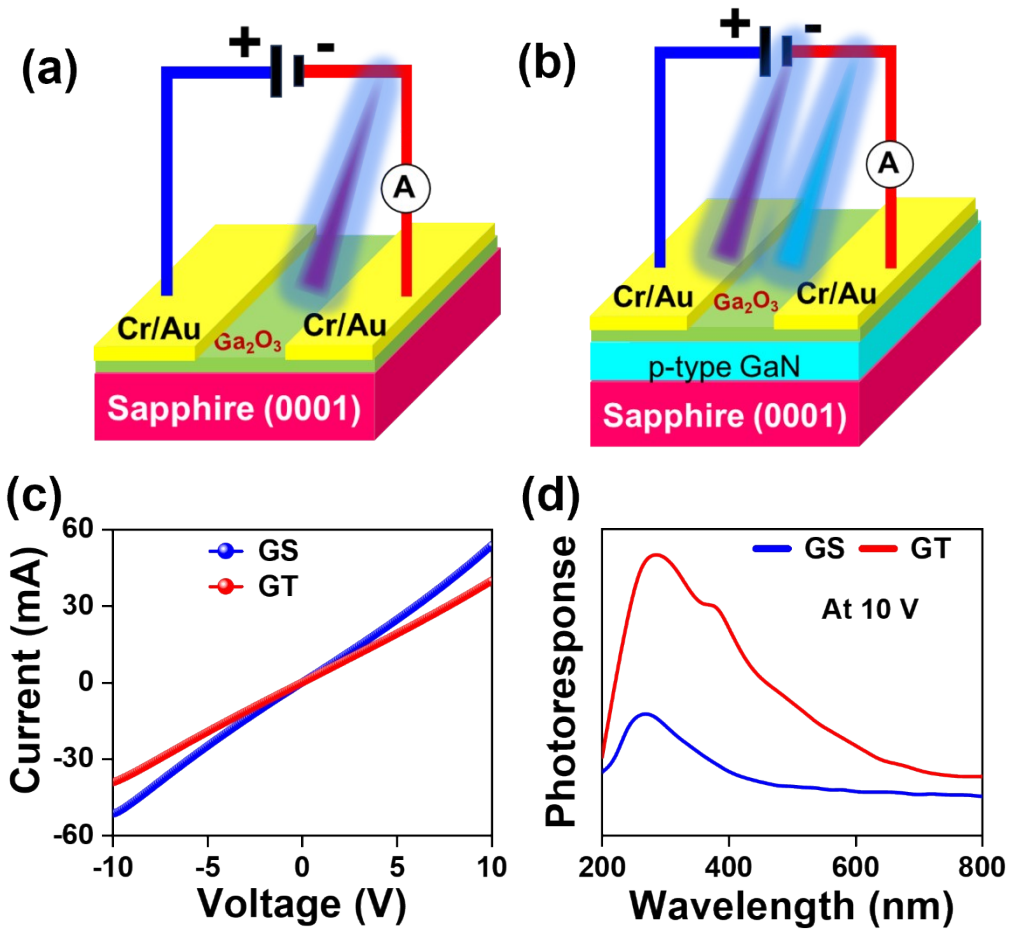

Figure S4: *Schematic diagram of PD device on samples (a) GS and (b) GT. (c) Current-voltage characteristics of both devices under dark and (d) Spectral response of both PD devices at 10 V in the 200-800 nm range.*

The I-V characteristics demonstrate that the PD device fabricated on sample GT has a lower dark current than sample GS. Further, we have performed each PD device's spectral photo response characteristics under illumination with a Xenon lamp in the wavelength region of 200 to 800 nm at 10 V, as shown in Figure S4(d). The spectral response of PD device on sample GS illustrates that the maximum photocurrent was observed to be in the wavelength region centered at 260-270 nm, i.e., in the DUV region, while that of PD device on samples GT gives the photocurrent in the not only DUV region but also UV-A region of wavelength of 355-365 nm. The presence of a photoresponse signal in the UV region reveals the active participation of p-GaN in PD device on samples GT. This implies that later PD can detect light in a broad UV region of the wavelength spectrum with high photoresponse, and hence, this finds its application in the UV C to UV A region.

We have conducted the AFM scans to examine the surface roughness of magnetron-sputtered $MoSe_2$ thin film deposited on PLD-grown β-Ga2O3 samples. Figures S5 (a) and S5 (b) show the AFM image with a scan area of $(2\ \mu m)^2$. The AFM images of both samples, MGS and MGT, complement the worm-like structures of magnetron-sputtered $MoSe_2$ thin film as depicted from FESEM images in Figures 4(c) and 4(d). The roughness of MGS and MGT

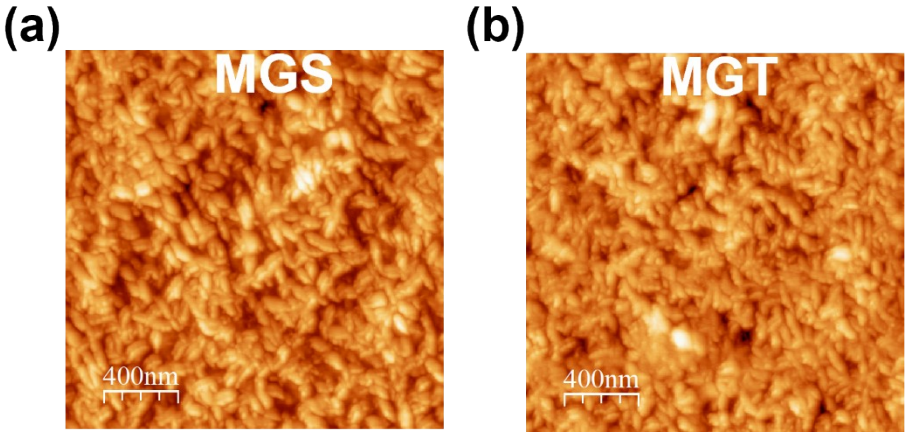

samples was estimated to be 7.37 and 5.42 nm, respectively.

Figure S5: *AFM images after deposition of sputtered $MoSe_2$ sample: (a) MGS and (b) MGT.*

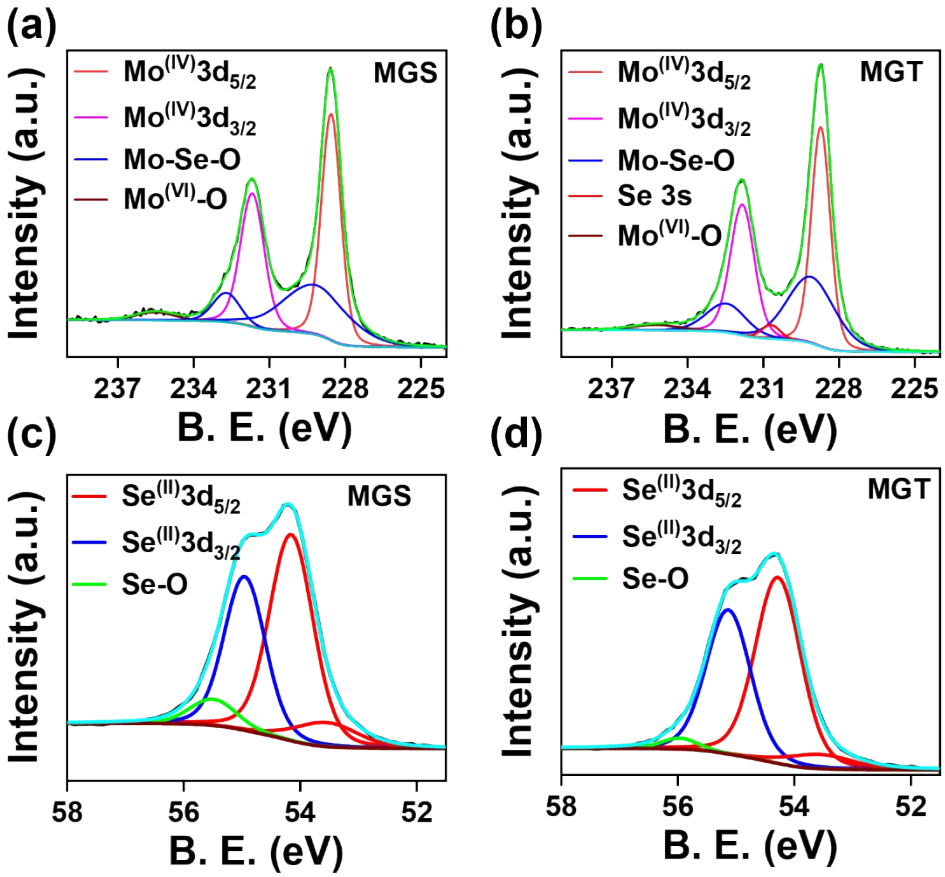

Figure S6*: Mixed Lorentzian-Gaussian function fitted XPS core level (a) and (b) Mo 3d scan of samples MGS and MGT, (c) and (d) Se 3d scan of samples MGS and MGT, respectively.*

Figures S6 (a) and S6 (b) show deconvoluted spectra of Mo 3d core level presenting different valence states of Mo element present on the surface of samples MGS and MGT, respectively. It shows the clear appearance of Mo and Se on the surface of the $MoSe_2$ film and confirms the formation of the 2H-$MoSe_2$ phase [4, 5]. The peaks at binding energies 228.5 (228.7) eV and 231.6 (231.8) eV for sample MSG (MGT) are related to spin-orbit coupled $3d_{3/2}$ and $3d_{5/2}$ subshell of the Mo atoms involved in the 2H-$MoSe_2$ phase [4]. For both samples, the peaks located at 235.7 eV are attributed to the 6+ valence state of Mo, while the Se 3s peak appears at 229 eV. [4] We also observed a Mo-Se-O peak, indicating some oxygen trash due to exposure from the environment during ex-situ XPS measurements [4, 5]. The Se 3d spectra of

$MoSe_2/Ga_2O_3$ are illustrated in Figures S6 (b & c). The peak position and FWHM of each deconvoluted peak are presented in Table S1.

Further, no peak corresponding to Mo-Ga [Figure S6 (a & b)] or Se-Ga [Figure S6 (c & d)] was observed in both the samples, which suggests that $MoSe_2$ is not attached to Ga_2O_3 by any chemical bonding but rather by weak van der Waals forces. Figure S6 (b & c) shows the Lorentzian-Gaussian function fitted Se 3d XPS scan of sample MGS and MGT. The Se 3d scan is deconvoluted to three peaks corresponding to spin-orbit coupled Se $3d_{3/2}$ (54.9 eV) and Se $3d_{5/2}$ (54.1 & 54.6 eV) [6], and in addition to this, a small peak appeared at higher binding which was found corresponding to Se-O. Further, the valence band spectra of sample MGS and MGT were plotted as shown in Figure S6 (d), which reveals that the valence band maxima lie 0.17 and 0.26 eV away from the fermi energy levels in samples MGS and MGT, respectively.

To understand the behavior of the fabricated devices under light, we performed the current-voltage (I-V) characteristics of each PD device under dark and light conditions in the voltage range of -10 to 10 V, as shown in Figure S7 (a & b). The current flowing through semiconducting material increases with an increase in applied voltage. This happens because the electric field experienced by the electrons inside the material also increases, leading to an enhancement in the drift velocity of charge carriers. Additionally, the electric field diminishes the recombination rate of charge carriers, which helps to improve the external circuit current. It has been observed that the current becomes higher at each voltage in the presence of light compared to the current measured in the absence of light (i.e., in dark conditions), as shown in the inset of Figures S7 (a & b).

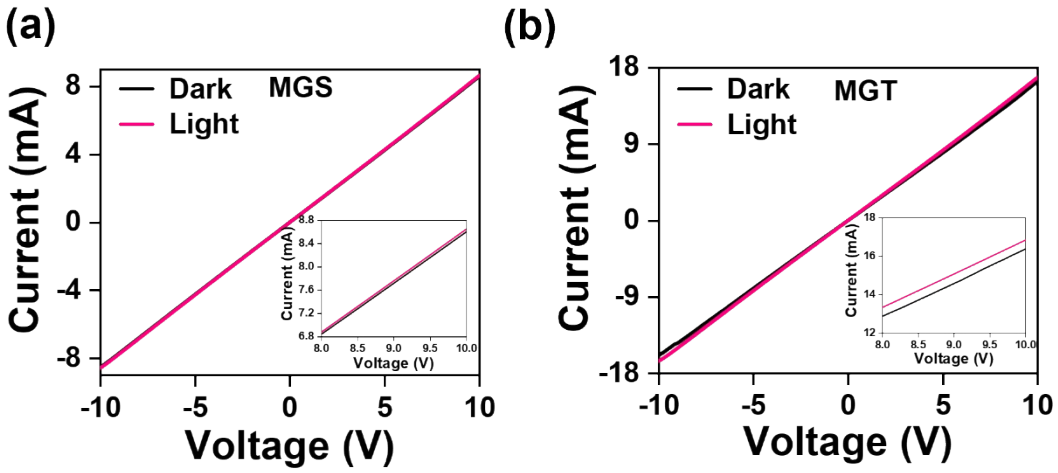

Figure S7*: Current-voltage characteristics under dark and light conditions of devices (a) MGS and (b) MGT.*

Table S1: Deconvoluted Peak Positions and their FWHM values for sample MGS and MGT.

Sample Index	The binding energy of peaks position (FWHM) in eV							
	Mo 3d					Se 3d		
	Mo $3d_{5/2}$	Mo $3d_{3/2}$	Se 3s	Mo-Se-O	Mo-O	Se $3d_{5/2}$	Se $3d_{3/2}$	Se-O
MGS	228.55 (0.90)	231.67 (1.10)	--	229.18 & 232.70 (3.06 & 1.25)	235.49 (1.80)	54.15 & 53.54 (0.88 & 1.25)	54.95 (0.82)	55.49 (0.93)
MGT	228.71 (0.88)	231.83 (1.08)	230.66 (0.79)	229.08 & 232.18 (2.23 & 2.08)	235.25 (2.26)	54.27 & 53.56 (0.91 & 1.31)	55.12 (0.89)	55.96 (0.72)

References:

1. J. Wei, K. Kim, F. Liu, P. Wang, X. Zheng, Z. Chen, D. Wang, A. Imran, X. Rong and X. Yang, β-Ga_2O_3 thin film grown on sapphire substrate by plasma-assisted molecular beam epitaxy. Journal of Semiconductors, 2019, **40**(1), 012802.
2. V. E. Meyers. Advancing Selective-Area Doping and Annealing Strategies for High-Conductivity p-Type (Al) GaN System: State University of New York at Albany; 2023.
3. S. S. Kushvaha, M. S. Kumar, A. K. Shukla, B. S. Yadav, D. K. Singh, M. Jewariya, S. Ragam and K. K. Maurya, Structural, optical and electronic properties of homoepitaxial GaN nanowalls grown on GaN template by laser molecular beam epitaxy. RSC Advances, 2015, **5**(107), 87818.
4. S. Kandar, K. Bhatt, N. Kumar, A. K. Kapoor and R. Singh, Nanoscale $MoSe_2$ Grown on Si (111) for Potential Applications in Broadband Photodetectors. ACS Applied Nano Materials, 2024, **7**(7), 8212.
5. G. S. Papanai, K. R. Sahoo, S. Gupta and B. K. Gupta, Role of processing parameters in CVD grown crystalline monolayer $MoSe_2$. RSC Advances, 2022, **12**(21), 13428.
6. H. M. Ahmad, S. Ghosh, G. Dutta, A. G. Maddaus, J. G. Tsavalas, S. Hollen and E. Song, Effects of impurities on the electrochemical characterization of liquid-phase exfoliated niobium diselenide nanosheets. The Journal of Physical Chemistry C, 2019, **123**(14), 8671.